Available online at www.sciencedirect.com
SCIENCE DIRECT®
Journal of Nuclear Materials 319 (2003) 15–23
journal of nuclear materials
www.elsevier.com/locate/jnucmat

Study on the mechanical properties and thermal conductivity of silicon carbide-, zirconia- and magnesia aluminate-based simulated inert matrix nuclear fuel materials after cyclic thermal shock

Y.W. Lee [a,*], S.C. Lee [a], H.S. Kim [a], C.Y. Joung [a], C. Degueldre [b]

[a] Korea Atomic Energy Research Institute, P.O. Box 105 Yuseong, Daejeon, South Korea
[b] Laboratory for Materials Behaviour, Paul Scherrer Institut, 5232 Villigen PSI, Switzerland

Abstract

Modification of thermo-mechanical properties of simulated (SiC) silicon carbide-, (ZrO_2) zirconia- and ($MgAl_2O_4$) spinel-based inert matrix nuclear fuels after cyclic thermal shock was analyzed in terms of Vickers hardness (H_V), fracture toughness (K_{IC}) and thermal conductivity. Three different simulated specimens were used for the experiment; a solid solution of yttria-stabilized zirconia and ceria (composition: $Er_{0.07}Y_{0.10}Ce_{0.15}Zr_{0.68}O_{1.915}$, 92.0% TD, specimen hereafter called Ce–ZrO_2), a CeO_2-dispersed Mg-spinel (composition: 15wt%CeO_2–$MgAl_2O_4$, 93.7% TD, specimen hereafter called Ce-spinel) and a CeO_2-dispersed silicon carbide (composition: 80.8 wt% SiC, 6.9 wt% Al_2O_3, 5.1 wt% Y_2O_3 and 5.0 wt% CeO_2, specimen hereafter called Ce–SiC), CeO_2 being surrogate materials for PuO_2. Cyclic thermal shock experiment and thermal conductivity measurements were simultaneously carried out by heating disc-shaped specimens up to maximum temperature ranging from 1073 to 1673 K and then cooling down to 343 K with Ar gas during 20–25 min. The Vickers hardness of the three different thermally shocked specimens showed nearly constant values with increasing number of cycles, except for the specimen heated at 1673 K. The K_{IC} values of the corresponding specimens increased with the increasing number of cyclic thermal shock at 1673 K. For Ce–ZrO_2 heated at 1673 K, however, it decreases considerably due to the combined effects of formation of second phase and modification of the matrix composition thereby. The calculated thermal conductivity of Ce-spinel decreases as the number of cycles in thermal shock increases in the temperature range between 1073 and 1673 K, and Ce–SiC slightly decreased with the number of cycles in cyclic thermal shock and the variations in thermal conductivity are almost the same for the temperature increases of 1073 and 1373 K, whereas, in Ce–ZrO_2, it remains nearly constant.

1. Introduction

Plutonium is an inevitable by-product of nuclear energy generation in the context of the current fuel technology. A long-term reprocessing strategy as well as recent decisions on the dismantling of nuclear weapons will give rise to excess in separated Pu stocks. Burning Pu produced in the power reactors is one of the options to solve the problems caused by this Pu surplus. In addition, the spent fuels discharged from the reactors contain several minor actinides (MAs; Np, Am, and Cm) and long-lived fission products (LLFP; Tc, I and Cs). Due to their radiotoxicity, MAs have to be separated (partitioning) from the high level waste (HLW) containing fission products for a long-term disposition, and destroyed to form non-radiotoxic and, if possible, stable nuclides (transmutation).

Responding to such needs and changes in fuel cycle options, extensive studies are focused on innovative

* Corresponding author. Tel.: +82-42 868 2129; fax: +82-42 868 8868.
E-mail address: ywlee@kaeri.re.kr (Y.W. Lee).

0022-3115/03/$ - see front matter © 2003 Elsevier Science B.V. All rights reserved.
doi:10.1016/S0022-3115(03)00128-4

fuels, in view of reducing the amount of nuclear wastes and/or nuclear materials containing the separated surplus Pu, the so-called Inert Matrix Fuel (IMF). A number of ceramic oxide fuels and oxide inert matrices including stabilized zirconia (e.g. $(Y,Zr)O_2$) [1] and spinel ($MgAl_2O_4$) [2] and non-oxide fuels and inert matrices such as silicon carbide (SiC) [3] have been investigated since the first Inert Matrix Fuel Workshop up to the present time.

Nuclear fuel materials generally undergo changes in various properties during their service as heat sources in nuclear reactors. These changes, which are caused by fission damage, mostly regard thermal and high-temperature mechanical properties, influence the whole fuel performance and, hence, their safe operation.

Stabilized zirconia ($Er_{0.07}Y_{0.10}Ce_{0.15}Zr_{0.68}O_{1.915}$), spinel ($MgAl_2O_4$) and silicon carbide (SiC) are considered as the most preferred candidates in the aspect of their behavior under irradiation. This study concerns the variation of the mechanical properties and thermal conductivity of simulated $(Y,Zr)O_2$-, $MgAl_2O_4$- and SiC-based simulated inert matrix fuels after cyclic thermal shocks in order to predict their thermal and mechanical behavior during reactor operation.

2. Experimental

2.1. Sample preparation

Simulated IMF with yttria-stabilized zirconia and $MgAl_2O_4$ spinel (with CeO_2 replacing PuO_2) were prepared from a mixture of ZrO_2–10at.%Y_2O_3–7at.%Er_2O_3– 15at.%CeO_2 (hereafter called Ce–ZrO_2) and MgO–Al_2O_3 (spinel)–15at.%CeO_2 (hereafter called Ce-spinel), respectively by the dry powder milling method [4]. Simulated IMF material with silicon carbide matrix was prepared from a mixture of 80.8 wt% SiC, 6.9 wt% Al_2O_3, 5.1 wt% Y_2O_3 and 5.0 wt% CeO_2 powder (hereafter called Ce–SiC) by wet powder ball milling in ethanol for 72 h. Pellet specimens for Ce–ZrO_2 of 9 mm in diameter and 8 mm long with a sintered density of 92% TD (Theoretical Density) have been obtained from the mixtures of commercially available chemical products, that were compacted with a pressure of 300 MPa followed by sintering at 1923 K in a flowing air atmosphere for 24 h. For Ce-spinel pellet specimens, the above powder mixture was compacted under the same conditions as the Ce–ZrO_2 and sintered at 1873 K in a flowing air atmosphere for 24 h. Pellet specimens for Ce–SiC of 7.5 mm in diameter and 10 mm long with 92% TD have been obtained by compaction with uni-axial hydraulic press with a pressure of 300 MPa followed by cold isostatic pressing (CIP) with 250 MPa and gas pressure sintering (GPS) at 2173 K in N_2 atmosphere for 1 h. Similar methods have been previously used for preparation of Ce-simulated MOX (UO_2–5wt%CeO_2) [5,6], whose relevant data were reported below for comparison [7]. For the thermal shock experiments, the pellets were horizontally sliced into discs of about 5 mm in thickness, ground and polished.

2.2. Characterization and microstructure observation

The polished surfaces of the discs were prepared for the observation of microstructural features, which were quantified with the aid of an image analysis system, Image-Pro Plus™, connected to an optical microscope.

2.3. Measurement and calculation of the mechanical properties

The Vickers hardness (H_V in GPa) was measured by a conventional Vickers indentation method and calculated from the expression [8]

$$H_V = 1852 \cdot F \cdot d^{-2}, \tag{1}$$

where F is the load (N) and d is the average length of the diagonals of the Vickers indents (mm).

The K_{IC} values (MPa $m^{1/2}$) were calculated by the Indentation Crack Length method, using the expression [9]

$$K_{IC} = 0.16 \cdot H_V \cdot a^{1/2} \cdot (c/a)^{-3/2}, \tag{2}$$

where a is half of the diagonal of the indent and c is half of the total length of the crack resulting from the indentation. For the K_{IC} calculations, the indentations were performed with a load of 500 g, applied during 15 s, and the crack lengths were measured from median crack types.

2.4. Cyclic thermal shock experiment and derivation of the thermal conductivity

For the thermal shock experiments, the prepared specimens and the reference sample of known thermal conductivity (UO_2 sintered pellet, 98.9% TD) were loaded with a thermocouple on the surfaces directed to the center and inserted into an insulated specimen holder that was installed in a specially designed gas quenching furnace, shown in Fig. 1. The specimens were maintained in the quenching furnace at a selected temperature for 30 min in an argon atmosphere to reach thermal equilibrium, and taken up to the part where the argon cooling jet and the IR sensors for measuring the surface temperatures of the specimen and reference sample are installed. Cyclic thermal shock experiments and thermal conductivity measurements were simultaneously carried out by repeatedly heating the specimens up to 1675 K and cooling down to about 345 K with Ar within 10–20 min, during which the temperatures of both sides of the

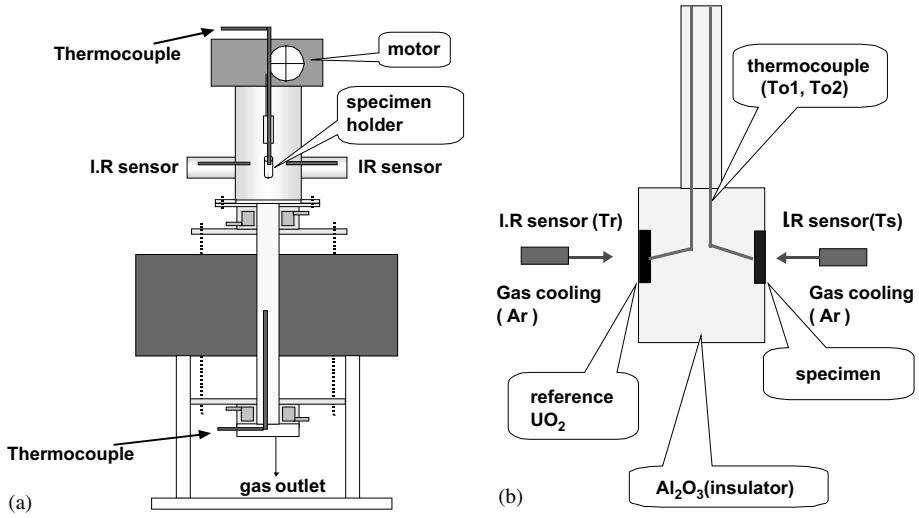

Fig. 1. Schematic diagram of the cyclic thermal shock device. (a) Thermal shock furnace and (b) specimen holder.

specimens and reference sample were recorded as a function of cooling time. This technique, developed recently in our laboratory [10], utilizes the difference between these temperatures to derive the thermal conductivity of the specimen as a function of temperature.

3. Results and discussion

3.1. Variation of the mechanical properties and microstructural modifications as a function of number of thermal shock cycles

For observing the variation of the mechanical properties of the specimens as a function of cyclic thermal shock, the temperatures of 1073, 1373 and 1673 K and 1, 5 and 10 cycles were selected. Fig. 2(a)–(c) show, respectively, the variations of density, Vickers hardness and fracture toughness of Ce–ZrO_2 specimens as a function of number of cycles at three different temperatures. For Ce–ZrO_2, the fracture toughness decreases at 1673 K after 10 thermal shocks. This is thought to be caused by formation of a monoclinic Ce–ZrO_2 phase, as witnessed by the X-ray diffraction analysis shown in Fig. 3.

Fig. 4(a)–(c) show, respectively, the variations of density, Vickers hardness and fracture toughness of the Ce-spinel specimens as functions of number of cycles at three different temperatures. As shown in Fig. 4(b) and (c), H_V and K_{IC} remain nearly constant as the number of cycle increases up to 10 at different temperatures. However, K_{IC} increases as the thermal shock temperature increases. This can be explained by density increase during cyclic thermal shock as shown in Figs. 4(a) and 7.

Figs. 5(a) and 2(b) show, respectively, variations of Vickers hardness (H_V) and fracture toughness (K_{IC}) of Ce–SiC specimens as a function of number of cycles at three different temperatures. Vickers hardness (H_V) does not vary significantly with the number of cycles in thermal shock in different temperatures, while fracture toughness (K_{IC}) increases with the thermal shock temperature, irrespective of the number of the cycles.

3.2. Observation of microstructural modifications after cyclic thermal shock

Fig. 6(a)–(c) compare optical micrographs of as-sintered, 1-cycle and 10-cycle thermally shocked Ce–ZrO_2 specimens at 1673 K, whose grains were revealed by chemical etching with an $NH_4F + 50\%H_2O$ solution at 110 °C for about 20 min. Fig. 6(d) is a macrograph of crack formation in the 10-cycles thermally shocked Ce–ZrO_2 specimen which evidences that a high thermomechanical stress is induced. Comparing the micrographs in Fig. 6(a)–(c), 1-cycle and 10-cycle thermally shocked Ce–ZrO_2 show a larger fractional porosity and better defined grains, entailing a decrease in microscopic density and hardness, respectively.

Fig. 7(a)–(c) compare optical micrographs of as-sintered, 1-cycle and 10-cycles thermally shocked Ce-spinel specimens at 1673 K, Fig. 7(d) shows crack formation in 10-cycles thermally shocked Ce-spinel, a behavior analogous to that of Ce–ZrO_2.

Fig. 8 compares optical micrographs of specimens as-sintered and 30-cycle thermally shocked at 1673 K in two different magnitudes. As can be seen in the micrographs, cyclic thermal shock does not induce any crack in Ce–SiC specimen at 1673 K even by 30 thermal shocks owing to the high thermal conductivity of the SiC

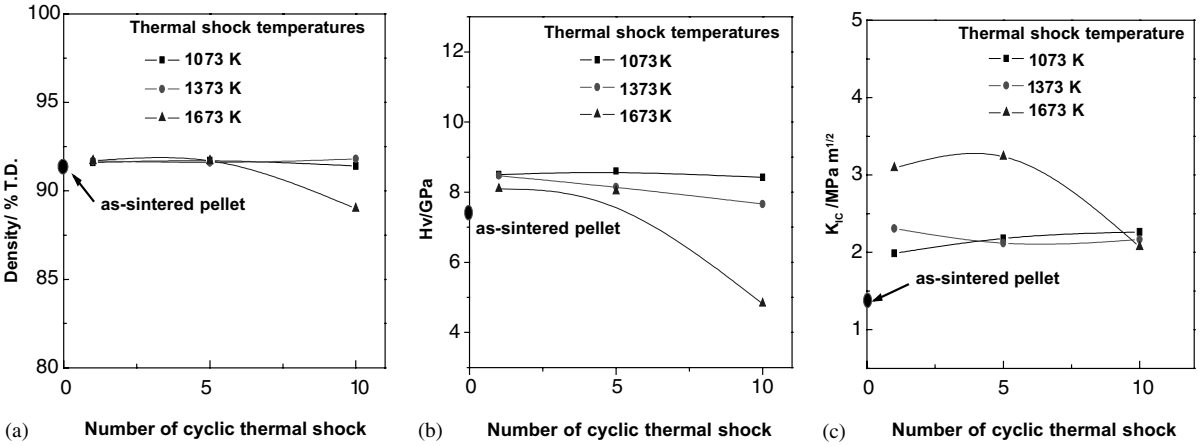

Fig. 2. The variation of the mechanical properties of Ce–ZrO_2 specimens as a function of the number of cycles in cyclic thermal shock. (a) Density variation, (b) Vickers hardness (H_V) and (c) fracture toughness (K_{IC}).

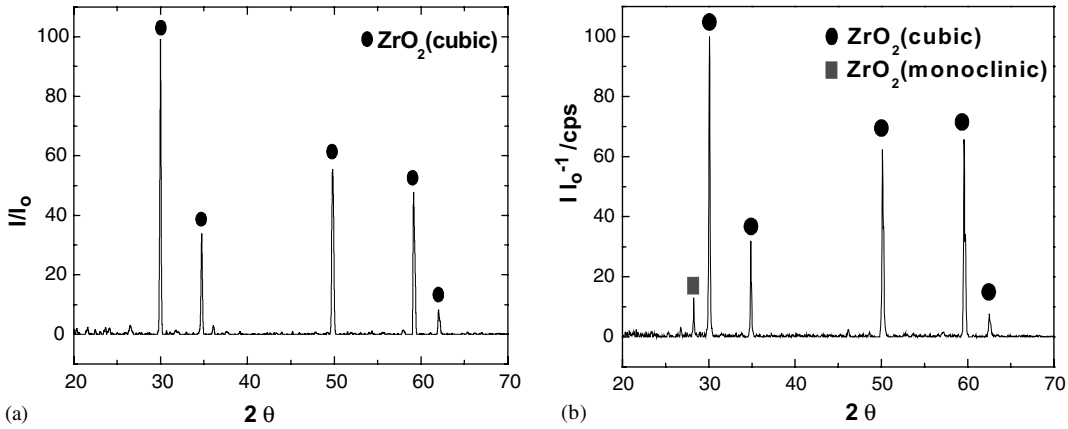

Fig. 3. XRD analysis results of Ce–ZrO_2 specimens (a) as-sintered and (b) after 10 cycles at 1673 K.

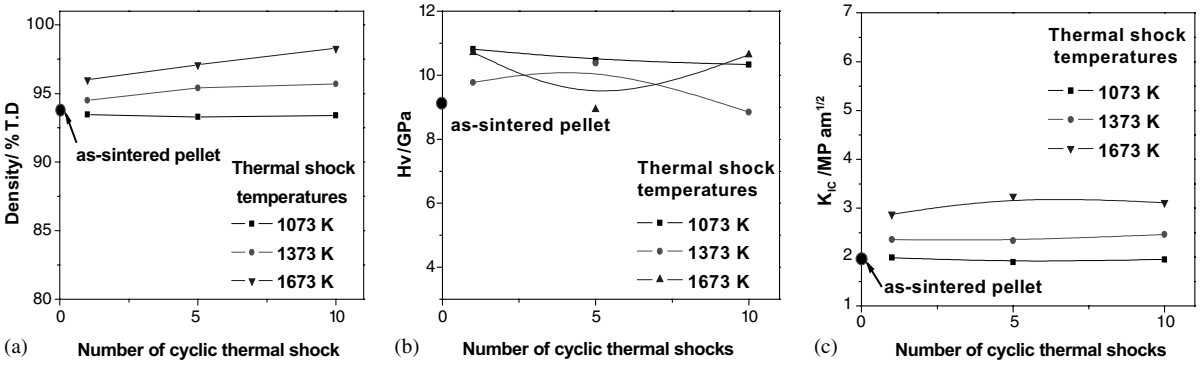

Fig. 4. The variation of the mechanical properties of Ce-spinel specimens as a function of number of cycles in cyclic thermal shock. (a) Density variation, (b) Vickers hardness (H_V) and (c) fracture toughness (K_{IC}).

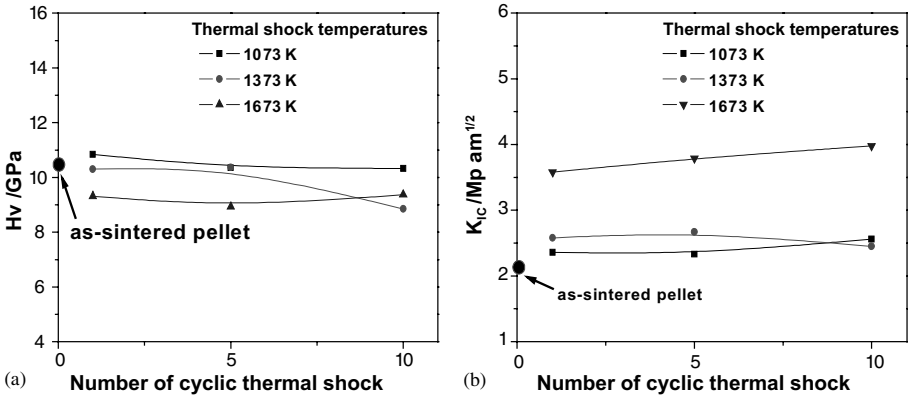

Fig. 5. The variation of the mechanical properties of Ce–SiC specimens as a function of number of cycles in cyclic thermal shock. (a) Vickers hardness (H_V) and (b) fracture toughness (K_{IC}).

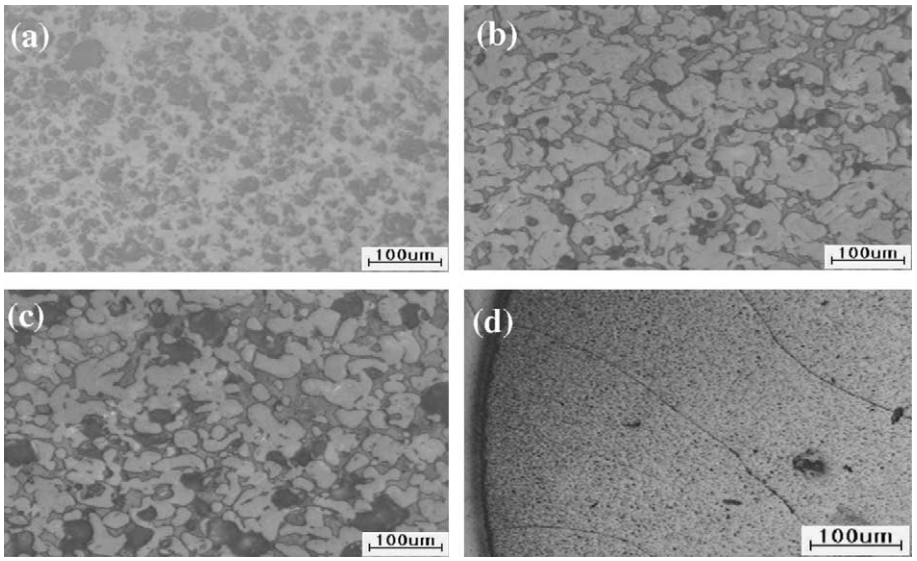

Fig. 6. The microstructural modification and crack formation in Ce–ZrO_2 specimens after cyclic thermal shock. (a) As sintered, (b) 1673 K/1 time, (c) 1673 K/10 times and (d) 1673 K/10 times crack formation.

matrix. However, cyclic thermal shock gives a decrease in density, hence an increase in porosity as shown in Fig. 8.

3.3. Thermal conductivity measurement and change in thermal conductivity after different numbers of cycles in thermal shock

For the measurement of the thermal conductivity and the observation of its change after different numbers of cycles in thermal shock, experiments were conducted only at 1673 K with 1, 10 and 30 cycles. Fig. 9 shows the change in thermal conductivity of Ce–ZrO_2 specimens as a function of temperature at different number of cycles in thermal shock, together with the result of Ce–ZrO_2 and Pu–ZrO_2 specimens measured at ITU [11]. Also shown, for comparison, are the data for Ce-MOX, measured by the same method compared with that measured by the laser flash method and Pu-MOX measured in ITU. It can be seen, that as the number of cycle increases the thermal conductivity slightly decreases. This can be attributed to the formation of cracks during cyclic thermal shock and density decrease as well. Compared with the data measured in ITU, the data in this work show higher values of about 1.0 $W m^{-1} K^{-1}$, attributed to the difference in the fabricated method. However, these are relatively in good agreement compared with other published data. Fig. 10 shows the change in thermal

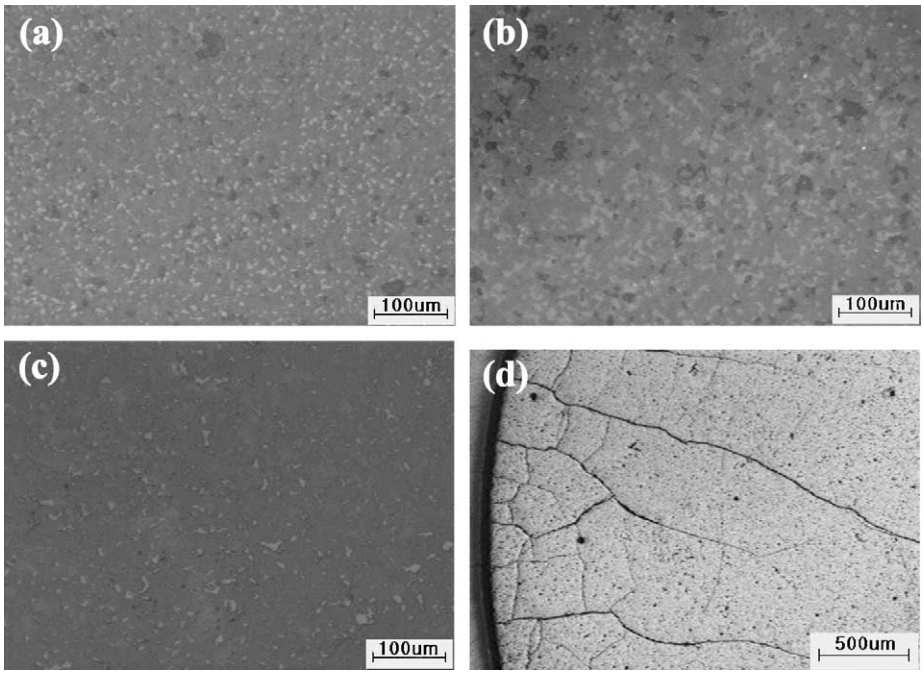

Fig. 7. The microstructural modification and crack formation of Ce-spinel specimens after cyclic thermal shock. (a) As sintered, (b) 1673 K/1 time, (c) 1673 K/10 times and (d) 1673 K/10 times crack formation.

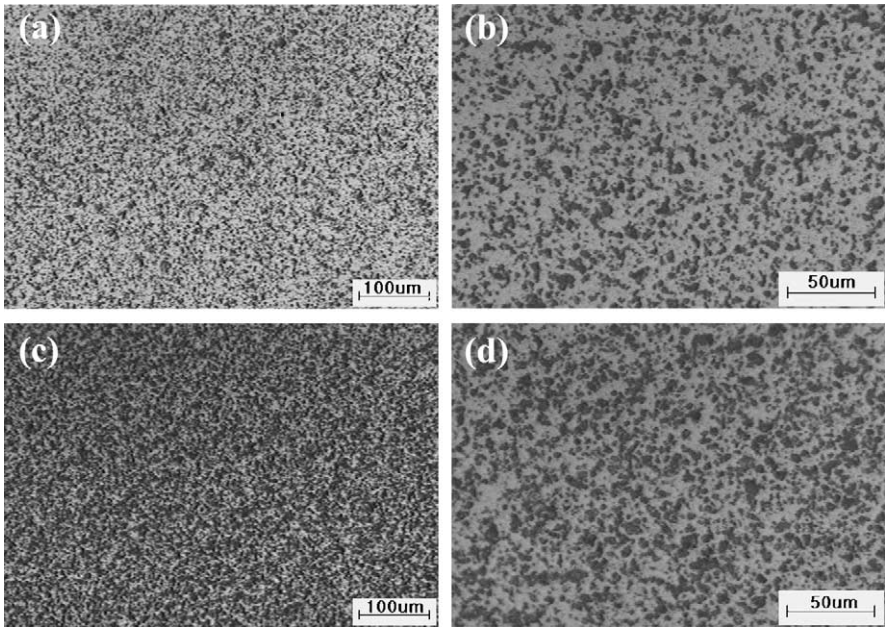

Fig. 8. The microstructural modification and crack formation of Ce–SiC specimens after cyclic thermal shock. (a) As sintered (×200), (b) as sintered (×500), (c) 1675 K/30 times (×200) and (d) 1675 K/30 times (×500).

conductivity of Ce-spinel specimens as a function of temperature at different number of cycles in thermal shock, together with the result of Mg-spinel specimens measured at NRG [12]. Also shown, for comparison,

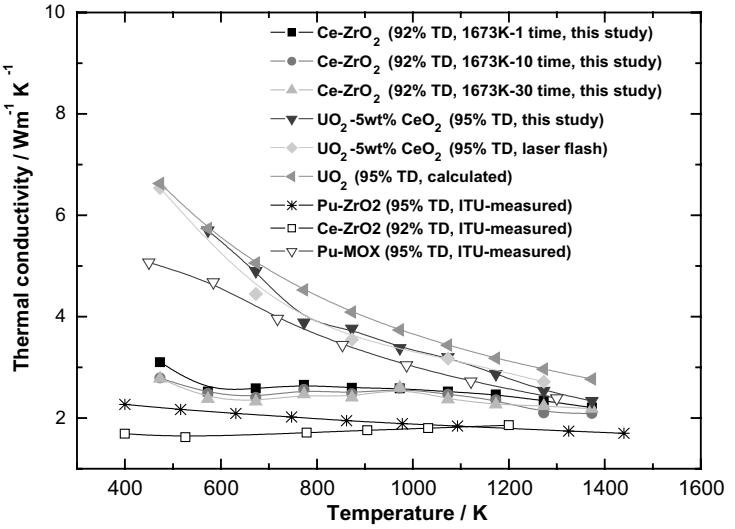

Fig. 9. Variation of the thermal conductivity of Ce–ZrO_2 as a function of thermal shock temperature and number of cyclic thermal shocks.

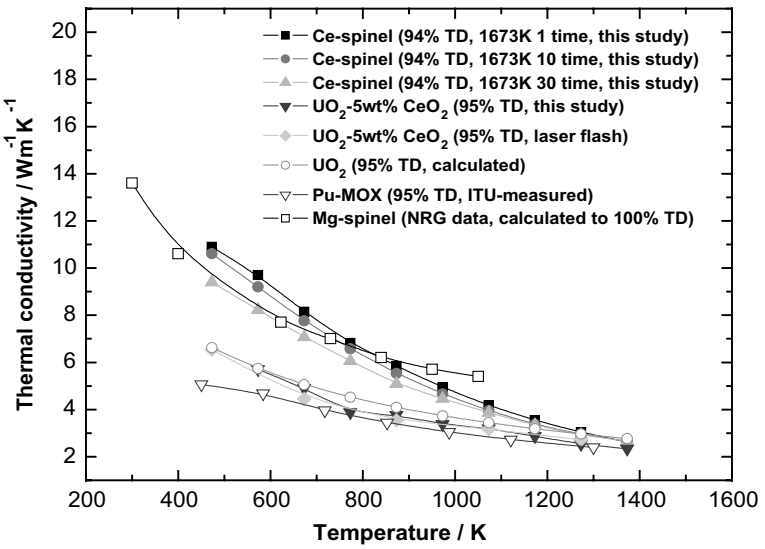

Fig. 10. Variation of the thermal conductivity of Ce-spinel as a function of thermal shock temperature and the number of cyclic thermal shock.

are the data for Ce-MOX, measured by the same method compared with that measured by the laser flash method and Pu-MOX measured at ITU. As it can be seen, as the number of cycle increases, the thermal conductivity in Ce-spinel decreases to a larger extent than in Ce–ZrO_2.

Fig. 11 shows change in thermal conductivity of Ce–SiC specimens as a function of temperature at different number of cycles in thermal shock, together with the result of 94% TD pure SiC specimen [3]. Also shown, for comparison, are the data for Ce-MOX, measured by the same method compared with that measured by Laser flash method and Pu-MOX measured in ITU [11]. As can be seen, as the number of cycle increases thermal conductivity decreases slightly. Also, Ce–SiC specimen shows higher thermal conductivity at the temperature

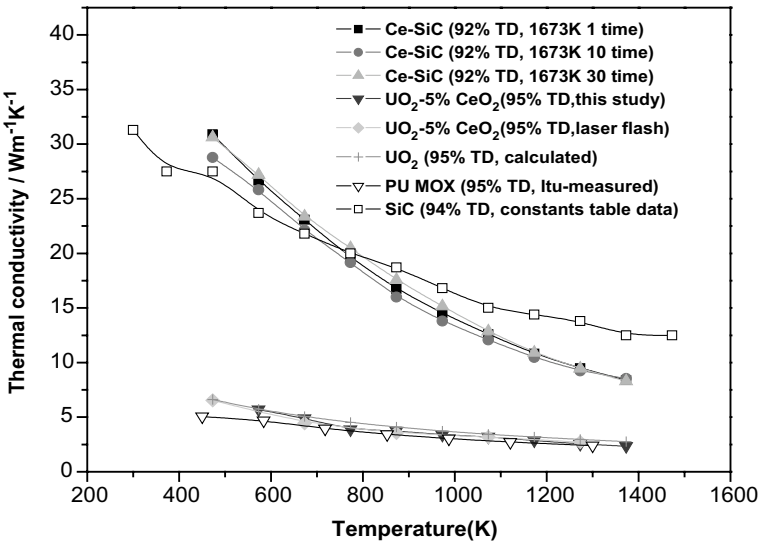

Fig. 11. The variations of thermal conductivity of Ce–SiC specimen as a function of thermal shock temperature and the number of cyclic thermal shock.

range of lower than 673 K and lower thermal conductivity at the temperature range between 673 and 1373 K.

4. Conclusions

From the obtained experimental results the following conclusions can be drawn:

(1) For the Ce–ZrO_2 IMF ($Er_{0.07}Y_{0.10}Ce_{0.15}Zr_{0.68}O_{1.915}$) pellet, its density, H_V and K_{IC} considerably decrease due to the formation of a monoclinic ZrO_2 phase, when 10 times thermally shocked at 1673 K.
(2) Vickers hardness (H_V) of the Ce–SiC does not vary significantly with the number of cycles in thermal shock in different temperatures, while fracture toughness (K_{IC}) increases with the thermal shock temperature, irrespective of the number of the cycles.
(3) The thermal conductivity values measured by the technique developed at KAERI [10] are in fairly good agreement with other published data.
(4) The thermal conductivity of Ce–ZrO_2 remains nearly constant in the temperature range between 473 and 1373 K.
(5) As the number of cycles increases the thermal conductivity of the Ce–ZrO_2 decreases slightly, this being attributed to the formation of cracks during cyclic thermal shock and possible density decrease as well.
(6) For the number of cycle increases, thermal conductivity of Ce–SiC specimen decreases slightly, and shows higher thermal conductivity at the temperature range of lower than 673 K and lower thermal conductivity at the temperature range between 673 and 1373 K. However, the conductivity of Ce-spinel decreases to a larger extent than that in Ce–ZrO_2 as the number of cycles increases.
(7) For both Ce–ZrO_2 and Ce-spinel, thermal shock at 1673 K by 10 times gives a crack formation due to thermo-mechanical stress. But cyclic thermal shock does not induce any crack in Ce–SiC specimen at 1673 K even by 30 times of the number of cycles, owing to the high thermal conductivity of the SiC matrix.

References

[1] G. Ledergerber, C. Degueldre, P. Heimgartner, M.A. Pouchon, U. Kasemeyer, Prog. Nucl. Energy 38 (2000) 301.
[2] K. Bakker, R. Belvroy, F.A. van den Berg, S. Casalta, R. Conrad, E.A.C. Neeft, R.P.C. Schram, W. Tams, Prog. Nucl. Energy 38 (2000) 313.
[3] R.A. Verrall, M.D. Vlajic, V.D. Krstic, J. Nucl. Mater. 274 (1999) 54.
[4] Y.W. Lee, H.S. Kim, S.H. Kim, C.Y. Joung, S.H. Na, G. Ledergerber, P. Heimgartner, M. Pouchon, M. Burghartz, J. Nucl. Mater. 274 (1999) 7.
[5] H.S. Kim, S.H. Kim, S.H. Na, Y.-W. Lee, J. Korean Nucl. Soc. 28 (1996) 458.
[6] K.S. Kim, Y.M. Kim, K.W. Kang, K.W. Song, J. Korean Nucl. Soc. 31 (1999) 608.
[7] S.C. Lee, H.R. Lee, Y.-W. Lee, in: Proc. of Korean Nucl. Soc. Spring Mtg., May 1999, p. 269.

[8] I.J. McColm (Ed.), Ceramic Hardness, Plenum, 1990.
[9] B.R. Lawn, E.R. Fuller, J. Mater. Sci. 10 (1975) 2016.
[10] S.C. Lee, H.S. Kim, Y.W. Lee, in: Proc. Korean Nucl. Soc. Spring Mtg., May 2002, p. 264.
[11] C. Ronchi, M. Sheindlin, Rpt. No. JRC-ITU-TPW-2001/008, 2001.
[12] R.J.M. Konings, K. Bakker, J.G. Boshoven, H. Hein, M.E. Huntelaar, R.R. van der Laan, J. Nucl. Mater. 274 (1999) 84.